CHAPTER 10

Lubricant-Impregnated Surfaces

BRIAN R. SOLOMON[a], SRINIVAS BENGALURU SUBRAMANYAM[a], TAYLOR A. FARNHAM[a], KARIM S. KHALIL[a], SUSHANT ANAND[a] AND KRIPA K. VARANASI*[a]

[a]Department of Mechanical Engineering, Massachusetts Institute of Technology, Cambridge, MA 02139, USA
*E-mail: varanasi@mit.edu

10.1 Introduction

Lubricant-impregnated surfaces (sometimes abbreviated to LIS) are composed of a liquid lubricant that is stabilized in a porous or textured solid by capillary forces.[1–5] Drops can exhibit high mobility and remarkably low contact angle hysteresis (<1°) on stable lubricant-impregnated surfaces. Many research groups have taken an interest in this technology and have expanded its use to many applications.

The following section outlines how to achieve a stable lubricant-impregnated surface and discusses its basic features including the wetting ridge and lubricant cloak. Next, applications of lubricant-impregnated surfaces are detailed including condensation, anti-icing, anti-fouling, fluid mobility, optics, and active surfaces. In each application, the design of a lubricant-impregnated surface has particularly relevant criteria. For example, cloaking of condensed water drops can adversely affect condensation heat transfer, and ice adheres more weakly to surfaces with more densely packed textures.

RSC Soft Matter No. 5
Non-wettable Surfaces: Theory, Preparation, and Applications
Edited by Robin H. A. Ras and Abraham Marmur

Published by the Royal Society of Chemistry, www.rsc.org

10.2 Fundamentals

A lubricant-impregnated surface is composed of a liquid lubricant that is stabilized in a porous or textured solid by capillary forces. The interface between a lubricant-impregnated surface and an immiscible liquid coming into contact with it (the working fluid) gives rise to many novel properties. If the system is properly designed (discussed below), the working fluid will not displace the lubricant. This section discusses the thermodynamics and the morphology of drops on lubricant-impregnated surfaces. It details how to achieve stability and important features such as the lubricant cloak and lubricant ridge that can form on working fluid drops.

Whereas a drop on a solid surface forms a single three-phase contact line between the liquid, air, and solid, the boundary between a working fluid drop and a lubricant-impregnated surface is more complex. Smith *et al.* describe the thermodynamics of drops on lubricant-impregnated surfaces and show that a drop on a lubricant-impregnated surface can exist in one of 12 different thermodynamic states depending on the properties of the working fluid droplet, impregnating lubricant, solid texture, and surrounding environment (see Figure 10.1).[5] The thermodynamic phase diagram is constructed

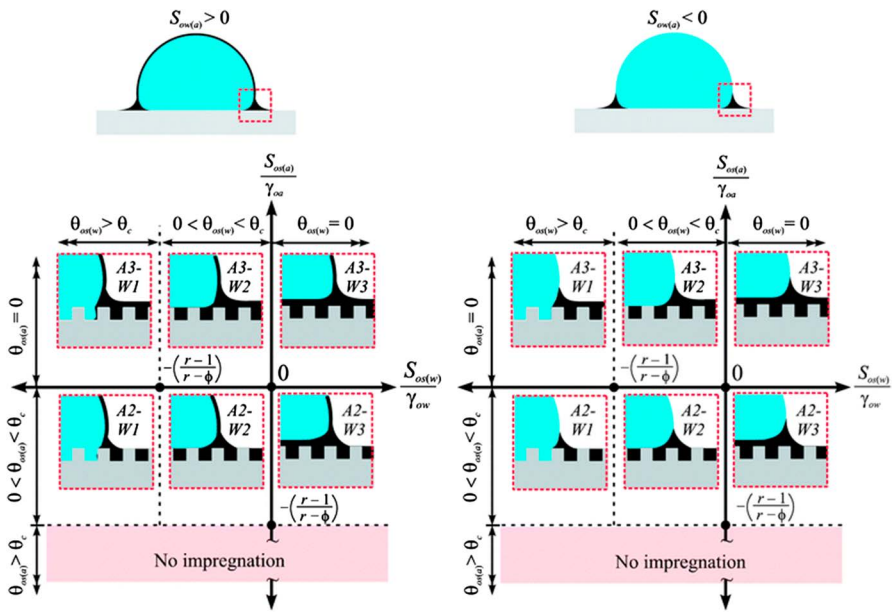

Figure 10.1 Possible thermodynamic states of a water drop placed on a lubricant-impregnated surface. The top two schematics show cases where the drop does and does not get cloaked by the lubricant. For each case, there are six possible states depending on how the lubricant wets the texture in the presence of air (the vertical axis) and the working fluid (horizontal axis). Reproduced from ref. 5 with permission from the Royal Society of Chemistry.

by considering the various possible configurations that are described below. Based on the properties of the materials involved (working fluid, lubricant, solid), three distinctly different morphologies of both the interfaces outside and underneath the drop are possible, as summarized in Table 10.1.[5] Considering the interface underneath the drop, in the first case, the working fluid displaces the lubricant, and the working fluid makes direct contact with the solid everywhere under the drop. This Wenzel-like state is referred to as the *impaled* state. In the second case, called the *impregnated*, *emerged* state, the lubricant remains contained in the solid and the working fluid contacts only the exposed features. In the third case, the working fluid makes no contact with the solid and sits on a thin equilibrium film (in contrast to an excess film[3]) of lubricant with its thickness set by the balance of intermolecular forces. This *encapsulated* state exhibits the most slipperiness (as quantified by the roll-off angle) whereas the impaled state, similar to the Wenzel state on a superhydrophobic surface, has poor slipperiness.[5]

These three distinct morphologies underneath a working fluid drop on a liquid-impregnated surface are quantified in terms of total interfacial energy (Table 10.1). The state with the lowest interfacial energy will be the one observed in steady state for a chosen working fluid, lubricant, and solid combination. The solid surface is characterized by the roughness r that denotes the total surface area of the solid per projected area, and the solid fraction ϕ denotes the fraction of the solid that makes contact with the working fluid in the impregnated, emerged state. Accounting for each interface beneath the drop gives the total interfacial energy per area of $E_{w1} = r\gamma_{sw}$ for the impaled state, $E_{w2} = (r - \phi)\gamma_{os} + \phi\gamma_{ws} + (1 - \phi)\gamma_{ow}$ for the impregnated, emerged state, and $E_{w3} = \gamma_{ow} + r\gamma_{os}$ for the encapsulated state. γ_{ij} denotes the interfacial tension between components i and j (w for working fluid, o for lubricant, and s for solid). The morphology with the lowest total interfacial energy per area will exist in steady state.

Equivalently, the encapsulated state is observed over the emerged state ($E_{w3} < E_{w2}$) when $S_{os(w)} = \gamma_{ws} - \gamma_{ow} - \gamma_{os} > 0$. Here $S_{os(w)}$ is the spreading coefficient of the lubricant (o) on the solid (s) in the presence of the working fluid (w). Spreading coefficients can be experimentally deduced by observing if a drop of lubricant spreads on a flat solid when in an environment of the working fluid. The drop size R should be small relative to the capillary length $\ell_c = (\gamma/\rho g)^{1/2}$ to ensure the spreading is not driven by gravity. Here, γ is the surface tension of the spreading liquid, ρ its density, and g is the gravitational acceleration.[6] Observing spreading of a lubricant indicates that $S_{ow(s)} > 0$ and the encapsulated state will exist for a textured solid of the same chemistry. These conclusions are summarized in Table 10.1.

As described by the above equations, lubricants and solids with low surface energies tend to form the most stable lubricant-impregnated surfaces. Oftentimes fluorocarbons (*e.g.* Krytox, FC-70), fatty alcohols (*e.g.* decanol), hydrocarbons, and silicone oils are used. Because evaporation of lubricant causes a lubricant-impregnated surface to lose its properties,[7] ionic liquids (*e.g.* BMIIm) have been proposed due to their extremely low vapour pressure

Table 10.1 Schematics of wetting configurations and interface energies. The total interface energies per unit area (column 3) are calculated for configurations outside and underneath a drop (column 2) by summing the individual interfacial energy contributions. Equivalent requirements for stability of each configuration are provided in column 4. In this table the lubricant is called "oil" and the working fluid is called "water".[a]

Interface	Configuration	Total interface energy per unit area	Equivalent criteria		
Oil-Solid-Air	*A1* Dry	$E_{A1} = r\gamma_{sa}$	$E_{A1} < E_{A2}, E_{A3}$	$S_{os(a)} < -\gamma_{oa}\left(\frac{r-1}{r-\phi}\right)$	$\theta_{os(a)} > \theta_c$
	A2 Impregnated, emerged	$E_{A2} = (r-\phi)\gamma_{os} + \phi\gamma_{sa} + (1-\phi)\gamma_{oa}$	$E_{A2} < E_{A1}, E_{A3}$	$-\gamma_{oa}\left(\frac{r-1}{r-\phi}\right) < S_{os(a)} < 0$	$0 < \theta_{os(a)} < \theta_c$
	A3 Encapsulated	$E_{A3} = \gamma_{oa} + r\gamma_{os}$	$E_{A3} < E_{A2}, E_{A1}$	$S_{os(a)} \geq 0$	$\theta_{os(a)} = 0$
Oil-Solid-Water	*W1* Impaled	$E_{w1} = r\gamma_{sw}$	$E_{w1} < E_{w2}, E_{w3}$	$S_{os(w)} < -\gamma_{ow}\left(\frac{r-1}{r-\phi}\right)$	$\theta_{os(w)} > \theta_c$
	W2 Impregnated, emerged	$E_{w2} = (r-\phi)\gamma_{os} + \phi\gamma_{sw} + (1-\phi)\gamma_{ow}$	$E_{w2} < E_{w1}, E_{w3}$	$-\gamma_{ow}\left(\frac{r-1}{r-\phi}\right) < S_{os(w)} < 0$	$0 < \theta_{os(w)} < \theta_c$
	W3 Encapsulated	$E_{w3} = \gamma_{ow} + r\gamma_{os}$	$E_{w3} < E_{w1}, E_{w2}$	$S_{os(w)} \geq 0$	$\theta_{os(w)} = 0$

[a]Reproduced from ref. 5 with permission from the Royal Society of Chemistry.

but tend to exist in the impregnated, emerged state rather than the encapsulated state.[5]

Porous or textured solids can either be inherently low-energy materials (*e.g.* PTFE membranes) or other materials (*e.g.* silicon, SU-8, aluminium) treated to be hydrophobic. Fabricating a texture for creating a lubricant-impregnated surface is identical to fabricating a texture to make a superhydrophobic surface. See Li *et al.*[8] and Roach *et al.*[9] for comprehensive reviews of superhydrophobic surfaces that include techniques to create textured surfaces. Researchers have successfully demonstrated lubricant-impregnated surfaces created by photolithography,[5,10] wet etching,[11–13] sol–gel synthesis,[14–18] layer-by-layer assembly,[19–22] and other techniques.[13,23–27]

A convenient way of filling a texture is to withdraw the textured or porous solid from a bath of lubricant. A lubricant will spontaneously wick into a texture provided its contact angle $\theta_{os(a)}$ on a smooth substrate of the same chemistry is below a critical angle. The critical angle θ_c is defined by $\cos\theta_c = (1-\phi)/(r-\phi)$ where ϕ is the solid fraction and r the total area divided by the projected area of a texture (Table 10.1).[1,28]

In withdrawing a substrate from a bath of lubricant, Seiwert *et al.* showed that a solid with well-defined micropillars entrains no excess lubricant provided the capillary number $Ca = \mu_o U/\gamma < 10^{-4}$ where μ_o is the viscosity of the lubricant, U is the withdrawal speed, and γ is the surface tension of the lubricant.[29] Such a dip-coating method is a popular technique to ensure the lubricant-impregnated surface has no excess film.

10.2.1 The Cloak

The lubricant can spread over the top of a working fluid drop and form a cloak (Figure 10.1). A cloak will form provided the spreading parameter of the lubricant on the working fluid in the presence of air (a) is greater than zero. Consideration of the cloak extends the possible morphologies of a drop on lubricant-impregnated surfaces to 12 possible states as shown in Figure 10.1.

The thickness of the lubricant cloak is set by a balance between the repulsive disjoining pressure and the Laplace pressure due to curvature. The Laplace pressure can be written as $2\gamma/R$ where γ is the surface tension of the lubricant and R the drop radius. The disjoining pressure $A_H/(6\pi h^3)$ is a function of the film thickness h and the Hamaker constant A_H which quantifies the interaction between air and working fluid molecules across the lubricant film. By balancing the Laplace pressure and disjoining pressure, Schellenberger *et al.* estimate that a cloak of the fluorocarbon FC-70 on a 1 mm drop of water is on the order of 20 nm thick.[10] Rykaczewski *et al.* and Anand *et al.* have confirmed cloaks over water drops by SEM,[30,31] and Schellenberger *et al.* have additionally confirmed the cloak by confocal microscopy (Figure 10.2).[32] Cheng *et al.* have also demonstrated high resolution X-ray tomography to visualize the water–lubricant interface.[33]

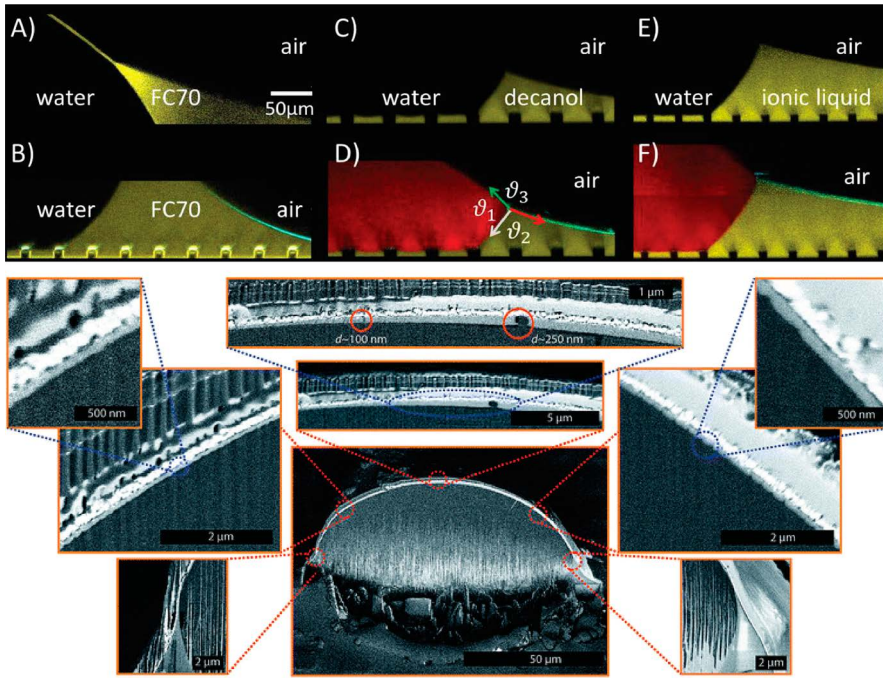

Figure 10.2 Cloaking of drops and the liquid–three-phase contact line. (top) Confocal images of vertical sections through a water drop placed on lubricant-impregnated micropillar array. FC70, decanol, and ionic liquid are used as lubricants. (bottom) Silicone oil cloak around a condensed drop suspended on a lubricant-impregnated surface obtained by a cryo-FIB-SEM process. The film is light grey sandwiched between the dark grey (water) and white (platinum). Reproduced from ref. 10 and 31 with permission from the Royal Society of Chemistry.

Anand *et al.* suggest that the formation of the cloak occurs in two steps.[31] First, a monolayer front spreads and its position follows $R = (4S_{ow(a)}/3(\mu_o\rho_o)^{1/2})^{1/2}t^{3/4}$ which is deduced from a balance between surface tension gradients and shear stress of the lubricant monolayer spreading on the liquid drop.[31,34] Next, a thicker film spreads. The relative scale of surface tension, viscous, and inertial forces in the spreading film is captured by the Ohnesorge number $Oh = \mu_o(\rho_o R\gamma_{oa})^{-1/2}$ where μ_o is the lubricant viscosity, ρ_o the lubricant density, R the working fluid drop radius, and γ_{oa} the lubricant surface tension. Carlson *et al.* observe that the time it takes a drop to detach from a needle when brought into contact with an oil film is $\tau_\rho = (\rho_o R^3/\gamma_{oa})$ for $Oh < 1$ and $\tau_\mu = \mu_o R/\gamma_{oa}$ for $Oh > 1$. These timescales give an estimate for the time it takes for the thicker film to completely cover the drop presuming detaching from the needle is a result of the complete spreading. Further work is needed to understand the dynamics of the spreading of liquids on liquids.

10.2.2 Wetting Ridge

When a working drop contacts a lubricant-impregnated surface, a ridge of lubricant forms around the drop[5] that is similar to ridges that can develop on soft solids.[35,36] Schellenberger *et al.* analysed the wetting ridge of several lubricant-impregnated surfaces (Figure 10.2).[32] They find that the height z of the wetting ridge follows from a balance between Laplace pressure and hydrostatic pressure, and its solution is a modified Bessel function of the second kind approximated by $z = \exp(-r/\ell_c)$ where r is the radial position and ℓ_c the capillary length. The wetting ridge is important because most of the viscous dissipation in a mobile drop occurs in the wetting ridge, as discussed later in this chapter.[5] Neeson *et al.* present a useful analysis on the morphology of drops with immiscible fluids that is relevant to drops on lubricant-impregnated surfaces.[37]

10.2.3 Excess Films and Steady State

At equilibrium, the configurations in which the tops of the solid texture underneath the drop is covered by a thin lubricant film (*e.g.* states *A3–W3* and *A2–W3* in Table 10.1) are only possible when the spreading coefficient $S_{os(w)}$ is positive. In all other cases the solid textures come into contact with the working fluid. The texture can be also overfilled,[3] however, as depicted in Figure 10.3. In addition, Schellenberger *et al.* demonstrated that overfilling

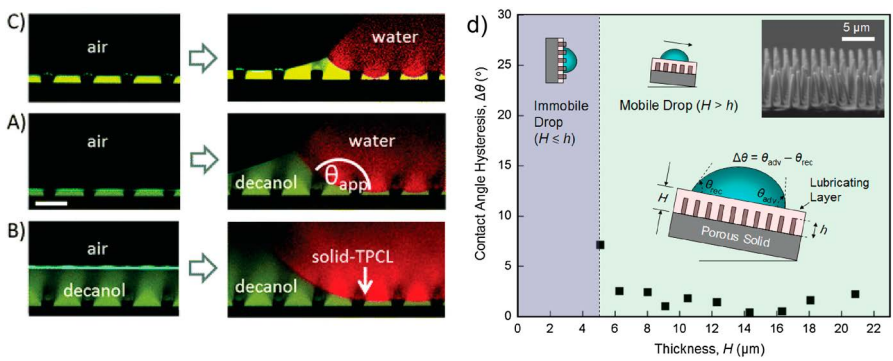

Figure 10.3 Influence of the filling height. (a–c) Image of a micropillar array infiltrated with decanol before and after a water drop is deposited. The height of the lubricant film is adjusted (a) to be underfilled, (b) to match the height of the posts, and (c) to be overfilled. Colour code: red, water; yellow/green, decanol; black, air or solid. Black shadows extend from the pillars because the sample was imaged from underneath. (d) Contact angle hysteresis of a 5 μL water drop on a lubricant-impregnated surface as a function of the lubricant height. (a)–(c) Reproduced from ref. 10 with permission from the Royal Society of Chemistry. (d) Reprinted by permission from Macmillan Publishers Ltd: *Nature*,[3] Copyright 2011.

a texture leads to different wetting ridge morphology,[32] and researchers have shown that the contact angle hysteresis of a water drop on a lubricant-impregnated surface as well as its sliding speed is significantly improved if an excess film is present.[12,38] While excess oil films may be beneficial (and also better in reducing ice adhesion[39]), the excess lubricant is not stabilized by capillary forces and can readily drain by gravity and other forces, thereby compromising slippery properties.

Carlson *et al.* demonstrate that a water drop can sit atop a thin oil film on a substrate for a finite time before the film drains in a system when the film drainage is favoured.[40] Similarly, drops on lubricant-impregnated surfaces may be mobile in transient states but behave differently once the lubricant-impregnated surface reaches its equilibrium state. The dip-coating method studied by Seiwert *et al.* and mentioned earlier in this chapter[29] is a convenient way to achieve a lubricant-impregnated surface with no excess lubricant.

10.3 Applications

10.3.1 Condensation

Approximately 40% of water usage worldwide is related to energy generation,[41] a demand primarily from power plants, most of which use steam cycles in their operation. A steam cycle comprises many components, but the condenser consumes the most water and contributes most to the overall steam cycle efficiency.[42] On a typical surface, steam condenses as a film that acts as a substantial thermal barrier to subsequent condensation (filmwise condensation). Alternatively, steam can condense as drops that roll off under gravity (dropwise condensation) and can provide up to a tenfold increase in heat transfer when compared to surfaces that condense filmwise.[42,43] Efforts have focused on superhydrophobic surfaces that exhibit extremely low droplet adhesion. However, these useful properties are lost during condensation because droplets nucleating randomly within textures of the solid can grow to large drops that may remain entrained within the textures in a Wenzel state (Figure 10.4a–c).

Lubricant-impregnated surfaces promote dropwise condensation. With a lubricant-impregnated surface, the lubricant contained in the surface prevents water from condensing within the texture (Figure 10.4e–f). In addition, the presence of the lubricant imparts exceptional mobility to condensed drops. On a conventional superhydrophobic surface, the critical size for drops to shed from the surface is on the order of a few millimetres (Figure 10.4g). On a lubricant-impregnated surface, Anand *et al.* observed that drops as small as 20 μm were mobile (speeds ~1 mm s^{-1}) on the surface (Figure 10.4g).[44] In addition, researchers have observed that under identical conditions, the onset of water condensation on lubricant-impregnated surfaces is faster than on superhydrophobic surfaces, suggesting

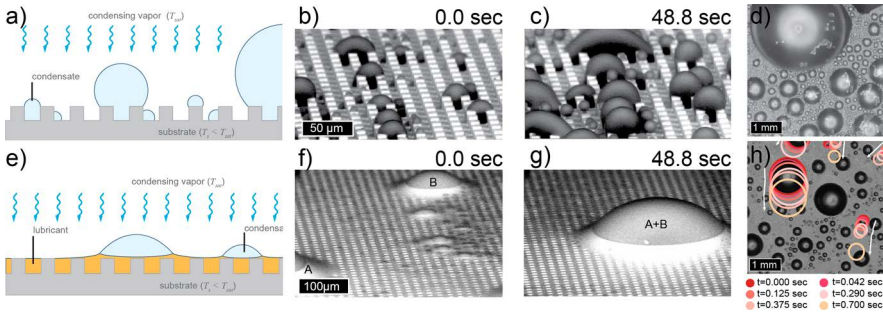

Figure 10.4 Comparison of condensation of water vapour on superhydrophobic (top row) and lubricant-impregnated surfaces (bottom row) with identical textures. (a) Schematic of condensation on superhydrophobic surfaces showing that water can nucleate within the texture and (b–c) timelapse ESEM images. (d) Drops grow and coalesce and eventually form large Wenzel drops that are pinned on the surface. (e) Schematic of condensation on lubricant impregnated surfaces showing condensation on top of the lubricant and (f–g) timelapse ESEM images. (h) Drops that condense and grow on a vertical lubricant impregnated surface are highly mobile. Reproduced with permission from Anand, S., Paxson, A. T., Dhiman, R., Smith, J. D. & Varanasi, K. K. Enhanced Condensation on Lubricant-Impregnated Nanotextured Surfaces. *ACS Nano* **6**, 10122–10129 (2012).[44] Copyright (2012) American Chemical Society.

that the lubricant-impregnated surfaces have a lower energy barrier for nucleation.[44,45]

The enhanced shedding and nucleation of drops indicates the potential of lubricant-impregnated surfaces for high condensation heat transfer. Xiao *et al.* quantify the condensation heat transfer of lubricant-impregnated surfaces as twice that of conventional hydrophobic and superhydrophobic surfaces in conditions comparable to those of industrial condenser operation (Figure 10.5a).[45] A lubricant-impregnated surface maintained dropwise condensation of steam up to the highest supersaturation tested whereas a superhydrophobic surface transitioned to filmwise condensation at high supersaturation.

Initially, Anand *et al.* had postulated that the nucleation of steam into water on lubricant-impregnated surfaces occurs at the lubricant–air interface,[44] whereas Xiao *et al.* had suggested that nucleation occurs at the solid surface beneath the lubricant.[45] In a later work, Anand *et al.* rationalize that water vapour has limited absorption into the lubricant and cannot achieve supersaturation to allow for nucleation within the lubricant, which suggest nucleation should occur only at the lubricant–air interface.[31] Further, they show that depending on the lubricant's surface tension and interfacial tension with water, nucleation on a lubricant can have a significantly lower energy barrier compared to that on solids. Based on such an analysis, they

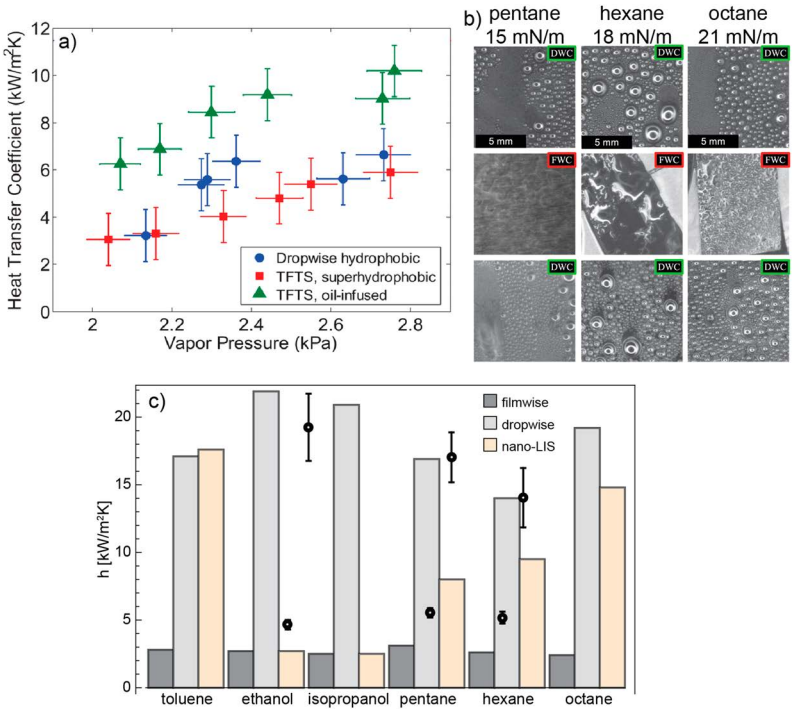

Figure 10.5 (a) Measured heat transfer coefficients for a flat hydrophobic surface, superhydrophobic surface, and Krytox-impregnated surface with varying vapour pressures. The Krytox-impregnated surface shows roughly twice the heat transfer of the other surfaces. (b) Images of the condensate of three low surface tension fluids on three different surfaces. Both dropwise condensation (DWC) and filmwise condensation (FWC) is observed. (c) Heat transfer coefficients for the condensation of low surface tension liquids on a flat silicon surface, a flat hydrophobic surface, and a Krytox-impregnated surface. Bars are generated from modelling whereas points indicate measured values. (a) Reprinted by permission from Macmillan Publishers Ltd: *Scientific Reports* (ref. 45), Copyright 2013. (b)–(c) Reprinted by permission from Macmillan Publishers Ltd: *Scientific Reports* (ref. 49), Copyright 2014.

constructed a regime to aid selection of lubricants that may lead to enhanced nucleation.[31]

Because condensers operate at low pressures, lubricants used for condensation applications must have low vapour pressure so that they are not rapidly lost. For condensation the existence of a lubricant cloak plays a special role. As discussed in Section 10.2, a lubricant can cloak over the top of a working fluid drop deposited on a lubricant-impregnated surface (Figure 10.2). The lubricant will cloak provided the spreading coefficient of the lubricant on the working fluid in the presence of air is positive ($S_{ow(a)} > 0$). Anand *et al.* show that the rate of condensed water drop growth on lubricant surfaces is significantly reduced on lubricants that form a cloak over the condensed water drops as compared

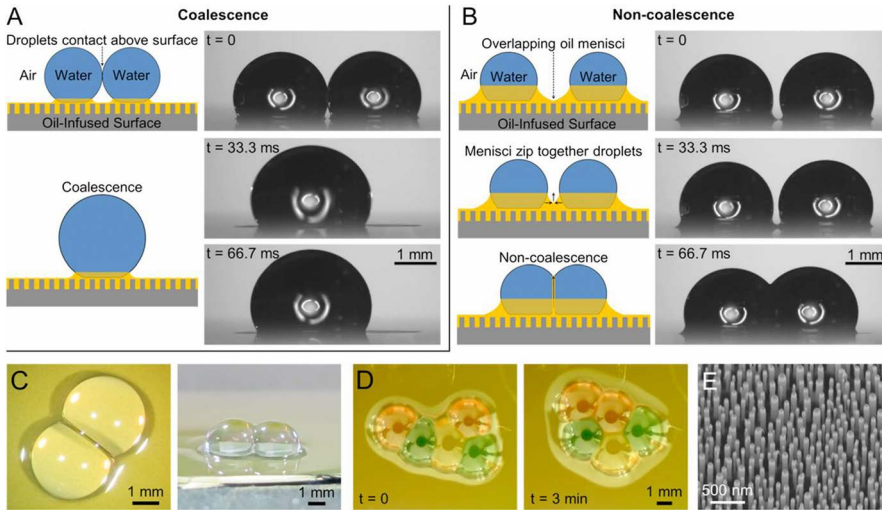

Figure 10.6 Interactive behaviour of water droplets on a lubricant impregnated surface. (a) Droplets colliding at the working fluid–air interfaces exhibited coalescence. (b) When the lubricant menisci of two drops overlap, a lubricant film formed between the droplets prevents coalescence. (c) Photographs of non-coalescing drops. (d) Multiple drops could be connected into a network. These networks spontaneously rearrange over time to minimize their surface energy. (e) SEM of nanopillared substrate. The oils used were (a,b) Krytox 100 and (c,d) Fomblin 25/6. Food colouring was used in (d). Reproduced from ref. 46 with permission of The National Academy of Sciences.

to those that do not. In a later work, Anand *et al.* show that a lubricant cloak forms almost immediately after water drops nucleate at the lubricant–air interface.[31] As a consequence, the capillary forces of the lubricant tend to submerge the drop after its formation. This prediction is confirmed by observing submerged microscopic droplets after condensation on a thin film of lubricant using a cryogenic focused ion beam (FIB)–SEM technique.

Figure 10.6 shows the non-coalescence of drops on a lubricant-impregnated surface. Boreyko *et al.* find that the non-coalescence is due to the lubricant wetting ridge.[46] Surprisingly, the time for two water drops to coalesce on a lubricant-impregnated surface is greater by an order of magnitude than for two water drops in a bath of the same lubricant, and increases with the lubricant viscsoity.[46] For example, the time for two 5 μL water drops to coalesce is roughly 1 day when the lubricant is 500 cSt silicone oil but only 1 s when the lubricant is 10 cSt silicone oil. Furthermore, they show that mixing phospholipids into the water drops creates lipid bilayers that prevent coalescence indefinitely. Barman *et al.* demonstrate that the coalescence process can be rapidly accelerated by applying a voltage between the two drops.[47]

Drops that condense and grow on a lubricant-impregnated surface with 1000 cSt silicone oil as the lubricant tend to grow in a narrow size distribution

whereas those that condense and condense on a lubricant-impregnated surface with 10 cSt oil tend to be more polydisperse.[31] While preventing coalescence can create controlled formation of condensed drops (which may find use in breath figure templating[48]), cloaking of water droplets by lubricant affects the longevity of lubricant-impregnated surfaces. Drops smaller than the solid texture features can submerge and displace lubricant. In addition, shedding of cloaked drops depletes lubricant. As a result, non-cloaking lubricants are more robust for condensation applications.

Rykaczewski *et al.* added to the body of literature on condensation on lubricant-impregnated surfaces to demonstrate the condensation of low surface tension liquids such as pentane and toluene (Figure 10.5b and c).[49] A variety of low surface tension liquids with surface tension ranging from 12 to 28 mN m^{-1} are tested on a lubricant-impregnated surface with Krytox as the lubricant and compared with flat and re-entrant textured oleophobic surfaces. Some liquids exhibited filmwise condensation on lubricant-impregnated surfaces as a consequence of displacement of Krytox by the condensing liquid, but most liquids exhibited sustained dropwise condensation. Up to an eight times increase in heat transfer resulted from promoting dropwise condensation of the low surface tension liquids.[49]

The condensation heat transfer discussed up until this point involves a vapour transitioning to a liquid when it cools. A related problem is the generation of water from fog comprised of liquid water drops (rather than water vapour) where phase change does not occur. The efficiency of fog collection is greatly dependent on the mobility of collected water drops on the collecting surface which can be improved by using lubricant-impregnated surfaces.[50] However, experiments on fog collection by Park *et al.* using Krytox-impregnated surfaces show gradual loss of lubricant with time.[51] Later, Boor *et al.* studied fog collection using superhydrophobic electrospun surfaces and compared fog collection with and without impregnated liquids.[52] Their results showed that a lubricant-impregnated surface with Krytox increased the water collection rate from fog as compared to a superhydrophobic surface by about 130%. Furthermore, they also investigated the leaching of oil from the surfaces and showed that the under their experimental conditions 3–5 μL of lubricant was detected per litre of collected water.

10.3.2 Anti-Icing

Lubricant-impregnated surfaces have been demonstrated as a passive means of reducing ice adhesion, which is a significant issue spanning multiple industries including transportation, agriculture, energy, and construction. Whereas superhydrophobic surfaces have been explored for anti-icing,[53,54] Varanasi *et al.* showed that frost that forms on superhydrophobic surfaces leads to strong ice adhesion.[55]

Kim *et al.* demonstrate reduced ice and frost adhesion and accumulation on a Krytox-impregnated surface with excess lubricant.[56] As shown in Figure 10.7, during frost tests the impregnated aluminium sample tilted at 75° show

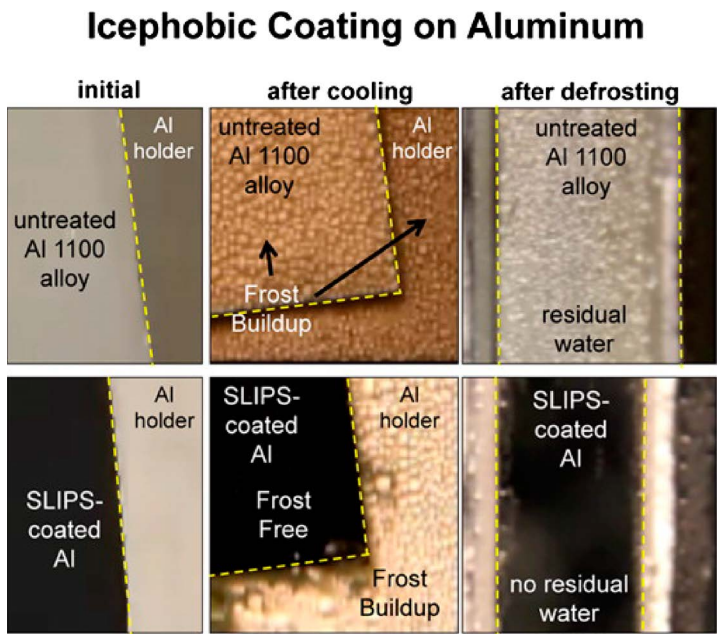

Figure 10.7 Comparison between an untreated aluminium 1100 sample (top) and lubricant-impregnated surface (bottom) comprised of textured alumina and Krytox. The samples were cooled to −10 °C at 60% relative humidity and defrosted at room temperature. Both samples are tilted at 75° for the duration of the experiment. Reproduced with permission from Kim, P. *et al.* Liquid-Infused Nanostructured Surfaces with Extreme Anti-Ice and Anti-Frost Performance. *ACS Nano* **6**, 6569–6577 (2012).[56] Copyright (2012) American Chemical Society.

no frost formation and no residual water after defrosting when compared to untreated samples. The lubricant-impregnated surface has less ice accumulation because condensed water can roll off easily at the 75° tilt angle before it freezes, and any accumulated ice easily rolls off the surface when defrosted. Additionally, measurements of ice adhesion strength show a reduction in adhesion strength of almost two orders of magnitude on surfaces with an excess lubricant film.

Subramanyam *et al.* extended these results by comparing a lubricant-impregnated surface with an excess film to one with an equilibrium film obtained by a controlled dip-coating process.[39] Compared to a lubricant-impregnated surface with excess lubricant, a lubricant-impregnated surface with the same texture and no excess lubricant shows higher ice adhesion (Figure 10.8). Optimizing the texture density of the lubricant-impregnated surface with no excess film results in lower ice adhesion than one of the lowest surface energy materials (80/20 PEMA-FluoroPOSS). Surprisingly, ice adhesion is lower on lubricant-impregnated surfaces that have higher texture densities. The researchers suggest that ice fractures more easily from

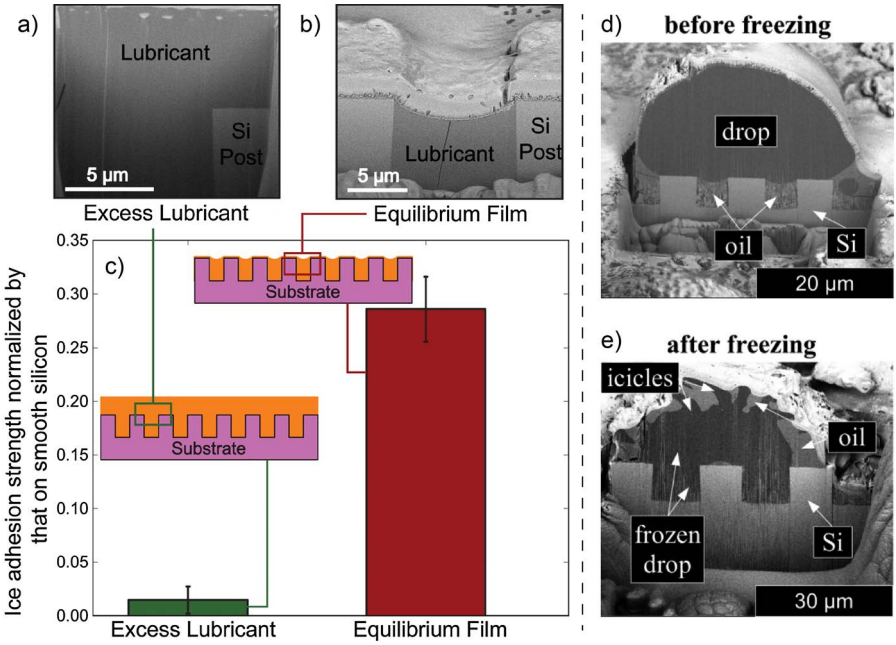

Figure 10.8 Cryo-SEM images of a cross-sectioned LIS with (a) excess lubricant and (b) no excess lubricant. (c) Comparison of the ice adhesion strength on LIS comparing excess and equilibrium lubricant films. The ice adhesion strength is normalized to that on a smooth, uncoated silicon surface. The textured surface of the LIS consists of lithographically textured silicon with 10 μm square posts with an edge-to-edge spacing of 50 μm. (d,e) Cross-section SEM images drops before and after freezing. The textured surface of Krytox-impregnated surface consists of lithographically textured silicon with 10 μm square posts with an edge-to-edge spacing of 10 μm. In the frozen drop the lubricant has migrated out of the texture and covers icicles. (a)–(c) Reproduced with permission from Subramanyam, S. B., Rykaczewski, K. & Varanasi, K. K. Ice Adhesion on Lubricant-Impregnated Textured Surfaces. *Langmuir* **29**, 13414–13418 (2013).[39] Copyright (2013) American Chemical Society. (d,e) Reproduced with permission from Rykaczewski, K., Anand, S., Subramanyam, S. B. & Varanasi, K. K. Mechanism of Frost Formation on Lubricant-Impregnated Surfaces. *Langmuir* **29**, 5230–5238 (2013).[122] Copyright (2013) American Chemical Society.

surfaces with higher texture densities because there is higher density of stress concentration sites.

Even with a lubricant in thermodynamic equilibrium, the lubricant can be depleted due to cloaking, solubility, evaporation, and other effects. In particular during ice and frost formation, Rykaczewski *et al.* show using cryogenic FIB-SEM that the lubricant can wick into icicles that accumulate on frozen water on lubricant-impregnated surfaces (Figure 10.8d and e).[57] When the ice is removed from the surface it takes lubricant with it. Depending on the selection of lubricant and texture, significant depletion can occur in just a

single frost–defrost cycle. Once the lubricant is depleted the ice adhesion will closely mirror the performance of the underlying superhydrophobic surface, which can be worse than that of an untreated surface.[55]

Accordingly, active research focuses on developing lubricant-impregnated surfaces for anti-icing with enhanced durability.[11,19,58,59] In one approach, Yin *et al.* introduce nanoparticles into the lubricant layer to selectively heat the lubricant-impregnated surface under near-infrared irradiation.[60] This allows for thermal deicing while still maintaining many of the benefits inherent in a lubricant-impregnated surface.

10.3.3 Anti-Fouling

10.3.3.1 Self-Cleaning

A surface from which contaminants such as dust can easily be removed by a liquid is referred to as a self-cleaning surface. Self-cleaning has been achieved using superhydrophilic surfaces that rely on film flow or using superhydrophobic surfaces with low contact angle hysteresis on which drops can easily roll off, taking contaminants with them.[61] Unfortunately, the durability of such surfaces to a wide range of contaminants and fluids limits their widespread use.

Lubricant-impregnated surfaces are well-suited for self-cleaning applications because of their extremely low contact angle hysteresis and ability to repel a wide variety of liquids.[50,59,62,63] Additionally, the angle at which a drop of a given size rolls off a lubricant-impregnated surface is much smaller compared to that on smooth, low surface energy solid materials. Furthermore, identically sized drops will have a larger area of contact on a lubricant-impregnated surface compared to a superhydrophobic surface, making lubricant-impregnated surfaces a useful tool for self-cleaning (Figure 10.9a).

The slippery nature of lubricant-impregnated surfaces also alters the drying pattern of droplets containing particles. Figure 10.9b shows a typical deposition pattern observed on a surface that has been called the "coffee ring effect." When an evaporating drop becomes pinned, particles migrate to the contact line and deposit forming a ring pattern. This behaviour is compared with the drying pattern of the same drop on a lubricant-impregnated surface. The lack of pinning during evaporation[64] on liquid-impregnated surfaces allows for a more uniform and localized deposition of particles.[50,62] Yang *et al.* have taken advantage of this effect to concentrate analytes in an evaporating liquid drop to improve Raman characterization.[65]

10.3.3.2 Biofilm Formation

Biofouling is widely prevalent in numerous industrial and medical applications. The formation of biofilms hampers the operation of marine vessels and desalination plants and can be catastrophic in catheter tubes and implants. Bacteria can also evolve to resist antimicrobial agents and hence

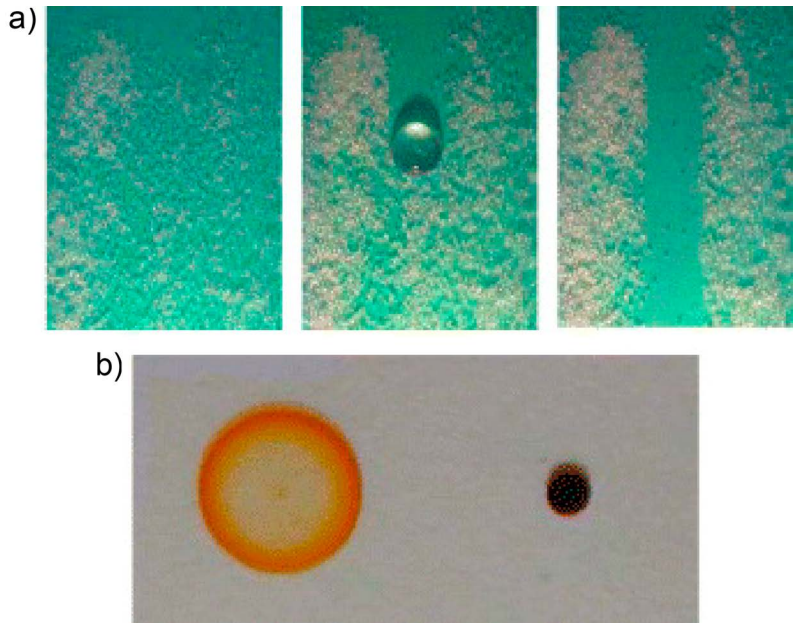

Figure 10.9 (a) A drop of water deposited on a silicone oil-impregnated surface cleans away silica dust particles. The surface is tilted at 20°. (b) Evaporated coffee drop on a plastic surface (left) in contrast to a coffee drop that evaporated on a silicone oil-impregnated surface. Reproduced with permission from *EPL*, 2011, 56001.[4]

other solutions are needed. The design of non-fouling surfaces has primarily focused on preventing protein adsorption and bacterial adhesion using functional groups including poly(ethylene glycol), zwitterions, and other hydrophilic groups that remain free of biofilm formation for only a limited time. Initial experiments showing lubricant-impregnated surfaces can repel blood and prevent bacterial attachment prompted further investigation into biofilm prevention.[63,66]

Epstein *et al.* showed that the slippery nature of lubricant-impregnated surfaces reduced bacterial accumulation and the overall adhesion of films under mild flow conditions.[67] Figure 10.10a compares the accumulation of *Staphylococcus aureus* on a PTFE substrate with a lubricant-impregnated surface. The lubricant-impregnated surface has 97.2% less bacteria after 48 h under flow. Similar reduction has been observed for *Escherichia coli*,[68] *Pseudomonas aeruginosa*,[68,69] and *Chlorella vulgaris*[70] as well as bacteria of the genus *Desulfovibrio*.[71]

Selective cell-repellency, which is important in biosensing and microfluidics, has also benefitted from liquid-impregnated surfaces. Ueda and Levkin have repelled cells into well-defined regions by patterning liquid-impregnated regions of a substrate.[72] Figure 10.10b shows fluorescent human cervical tumour cells separated by lubricant-impregnated regions in which cells cannot attach.

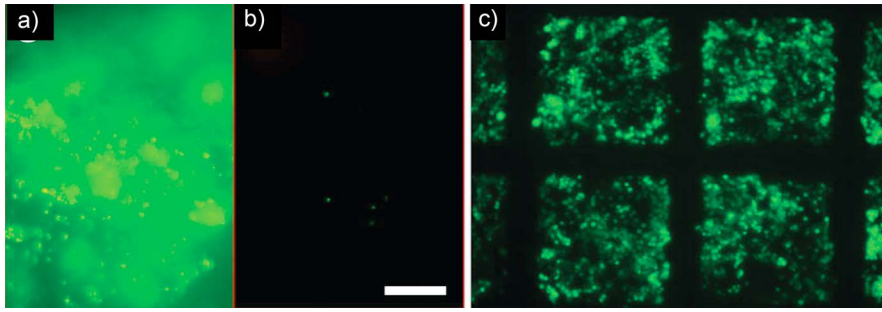

Figure 10.10 *Staphylococcus aureus* bacteria attachment (a) to a PTFE substrate and (b) to a lubricant-impregnated surface. Scale bar is 30 μm. (c) Selective repellency of human cervical tumour cells from the hydrophobic liquid barriers and preferentially attachment to the square hydrophilic areas. The width of each square well is 500 μm. Reproduced with permission from Epstein, A. K., Wong, T.-S., Belisle, R. A., Boggs, E. M. & Aizenberg, J. Liquid-infused structured surfaces with exceptional anti-biofouling performance. *Proc. Natl. Acad. Sci.* (2012). doi:10.1073/pnas.1201973109.[67] (c) Reproduced from ref. 72 with permission from John Wiley and Sons. Copyright © 2013 Wiley-VCH Verlag GmbH & Co. KGaA, Weinheim.

In marine vessels fouling can also occur from plants and animals that adhere to the hull. Xiao *et al.* investigate the attachment and adhesion of motile spores of the seaweed *Ulva linza*.[69] After 2 h, the number of *U. linza* spores that had attached to a Krytox-impregnated surface is significantly lower than for a control glass surface. The spores that attach have comparable adhesion strength to those on glass, however, as indicated by their resilience in staying attached under a shear water flow. In separate assays, these authors also demonstrated that the coverage of the larvae of the barnacle *Balanus amphitrite* was up to an order of magnitude less on Krytox-impregnated surfaces than on glass or polystyrene.

10.3.3.3 Scale Fouling

Fouling and corrosion of heat exchangers, oil and gas pipelines, and turbine systems lead to increased maintenance and losses in production. For heat exchanger scaling alone, the costs associated with operational losses, energy requirements, and maintenance is on the order of 0.25% of the GDP of industrialized countries.[73] Mechanical and chemical cleaning methods are economically or environmentally expensive. Low surface energy coatings have been shown to provide a passive route for limiting the fouling of surfaces but lack robustness in harsh conditions.

Liquid-impregnated surfaces are promising as a robust alternative to other low surface energy coatings. Reducing the nucleation rate of scale requires a lower density of nucleation sites and a high activation barrier. A low surface tension liquid entrained within the solid texture offers a molecularly smooth surface with a large activation barrier that can be used to lower

the nucleation rate. Figure 10.11a and b shows a comparison between an untreated surface and a silicone oil-impregnated surface immersed in a gypsum (calcium sulfate) solution for >3 days.[74] Subramanyam *et al.* showed that an optimal design with respect to the liquid surface tension and spreading coefficient can result in up to ten times lower scale formation on the impregnated surface compared to an untreated surface.[74] They also show that lubricant-impregnated surfaces can be fabricated on steel, which is used in industrial applications. Charpentier *et al.* extended this work to show a ten times decrease in scale deposits of calcium carbonate on liquid-impregnated surfaces.[75]

The corrosion of a material can also be slowed down with a liquid-impregnated surface. The use of superhydrophobic surfaces in marine environments to lower corrosion rates has limited success because, over time, the trapped air is lost. Figure 10.11c compares the corrosion of bare steel, hydrophobic steel, and a liquid-impregnated steel with varying amounts of infused liquid after 3 days of immersion in 3.5% NaCl solution.[76] On

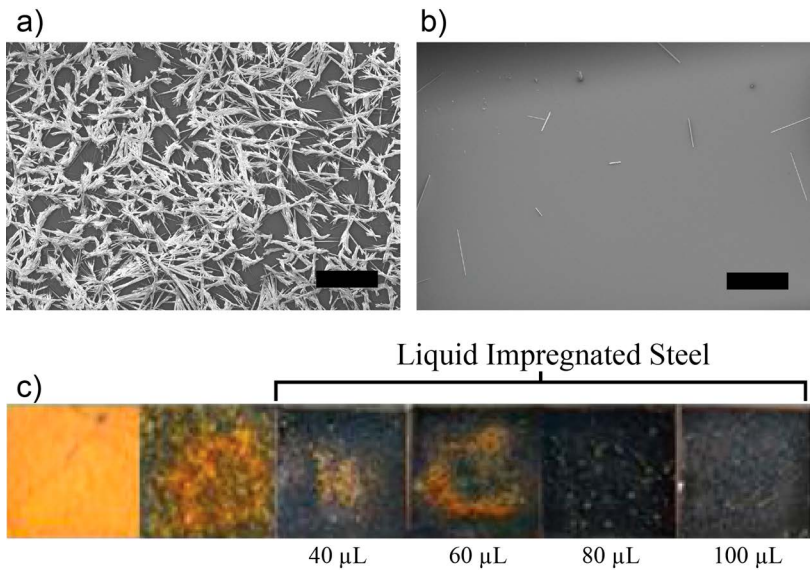

Figure 10.11 Gypsum scale formation after 80 h in a salt solution on (a) an untreated smooth silicon surface (b) a silicone oil-impregnated surface. Scale bar is 1 mm. (c) The corrosion of low alloy steel after 3 days of immersion in 3.5 wt% NaCl solution. From left to right: bare steel, hydrophobic steel, lubricant-impregnated steel where the volume of lubricant is varied. Reproduced from ref. 74 with permission from John Wiley and Sons. Copyright © Wiley-VCH Verlag GMbH & Co. KGaA, Weinheim, and reprinted from *Applied Surface Science,* **328**, S Yang *et al.*, Slippery liquid-infused porous surface based on perfluorinated lubricant/iron tetradecanoate: Preparation and corrosion protection application, 491–500, Copyright 2015 with permission from Elsevier.[76]

the liquid-impregnated surface, the perfluoropolyether lubricant acts as a protective layer and lowers the corrosion rate. Song *et al.* further quantify this corrosion resistance using electrochemical impedance spectroscopy to show that lubricant-impregnated surfaces do not corrode even after 76 days immersed in 3.5 wt% NaCl.[77,78]

10.3.4 Fluid Mobility

A drop placed on a lubricant-impregnated surface is mobile at very low angles. Smith *et al.* concluded that drops roll on lubricant-impregnated surfaces rather than slide, by balancing shear forces in the lubricant film beneath a drop and those within a drop.[5] Looking at the lubricant–working fluid interface beneath a drop on a lubricant-impregnated surface, the shear forces on the lubricant side scale as $\mu_o V_i/t$ where μ_o is the lubricant viscosity, V_i the interface velocity, and t the lubricant film thickness beneath the drop. The shear stress on the working fluid side scales as $\mu_w(V - V_i)/h_{cm}$ where μ_w is the working fluid viscosity, V the velocity of the centre of mass of the drop, and h_{cm} the height of the centre of mass. At the interface the shear stresses must balance, giving $V_i \sim V(1 + \mu_o h_{cm}/\mu_w t)^{-1}$. For the experiments of Smith *et al.* $V_i \ll V$, which indicates that the drop rolls. They confirm the rolling motion of the drop using tracer particles (Figure 10.12c).

Next, the speed of a drop in steady state on an inclined lubricant-impregnated surface is determined by balancing gravitational, pinning, and viscous forces. There are three possible regions of viscous dissipation resisting a drop's motion: in the rolling drop, in the lubricant beneath the drop, and

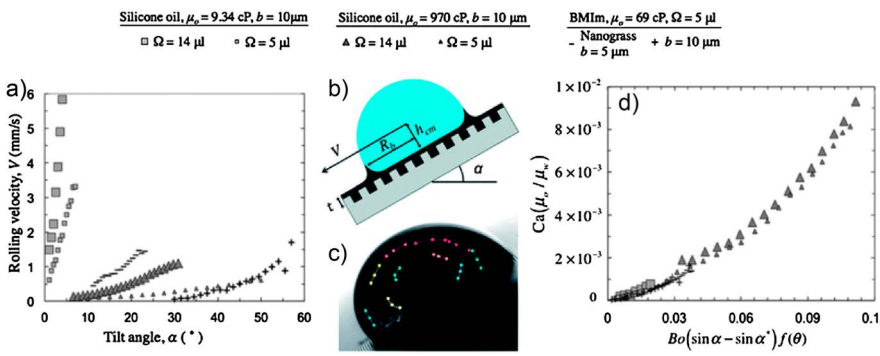

Figure 10.12 (a) Measured velocities of water droplets as a function of substrate tilt angle for various lubricant viscosities, textures, and drop sizes. (b) Schematic of a water droplet moving on a lubricant-impregnated surface showing the various parameters of consideration. (c) Trajectories of tracer particles measured relative to the water droplet reveal that the drop rolls rather than slides on LIS. (d) Non-dimensional plot collapsing the datasets shown in (a) onto a single curve. Reproduced from ref. 5 with permission from the Royal Society of Chemistry.

in the wetting ridge. For a water drop on a silicone oil-impregnated surface with no excess film, Smith *et al.* show that dissipation in the wetting ridge is the most dominant term and explains observed velocities for a wide range of lubricants, tilt angles, and drop sizes (Figure 10.12d).[5]

Abstracting away from drop level experiments, introducing a slippery surface has many applications in established industries. Slip in the walls of a pipe, for example, will increase the flow rate or decrease the power required to pump a fluid.

At a fluid–solid interface the most universally accepted boundary condition is no-slip, meaning the velocity of the fluid and solid must be matched. The no-slip condition has been experimentally validated under most normal flow conditions.[79] The interface between a lubricant-impregnated surface and working fluid requires special consideration, however, because the working fluid interfaces with either only the lubricant or a combination of lubricant and solid. In such a situation an apparent slip can arise although no-slip can still hold microscopically.

Such drag reduction has been studied for superhydrophobic surfaces by modelling the air–working fluid interface as shear free. Several studies have extended such work to incorporate the viscosity of air into models.[80–82]

While lubricant-impregnated surfaces are more stable than superhydrophobic surfaces and can repel a wider variety of liquids, lubricant-impregnated surfaces should provide less drag reduction than superhydrophobic surfaces since the viscosity of the lubricant is greater than that of air. Solomon *et al.* use a rheometer to measure the drag reduction on lubricant-impregnated surfaces in laminar flow with varying working fluid viscosities and attained a drag reduction of 16% in a 1 mm geometry when the working fluid was 260 times more viscous than the lubricant (Figure 10.13a).[83] Jacobi *et al.* point out that such measurements involving two immiscible fluids in a rheometer can be subject to an interfacial distortion that can contribute to the torque measurement.[84]

Schönecker *et al.* analytically investigated the drag reduction of lubricant-impregnated surfaces in laminar flow and found that a working fluid to lubricant viscosity ratio of 56 (consistent with water on a superhydrophobic surface) can attain a 20% flow increase on an optimized lubricant-impregnated surface (Figure 10.14). In comparing the flow enhancement when using lubricant-impregnated surfaces, the reference plane must be carefully chosen. For example, adding a lubricant-impregnated surface to the inner surface of a pipe reduces the radius. The advantages of a lubricant-impregnated surface would have to be greater than the added resistance of a decreased pipe radius.

Rosenberg *et al.* extended findings on drag reduction to higher Reynolds numbers.[85] Using a Taylor–Couette geometry they measure 10% drag reduction on superhydrophobic surfaces and 14% drag reduction on a heptane-impregnated surface which was constant over the Reynolds number range 7000–9000 (Figure 10.14b). Other work suggests that drag reduction can also be achieved in turbulent flows on lubricant-impregnated surfaces,[86] as has

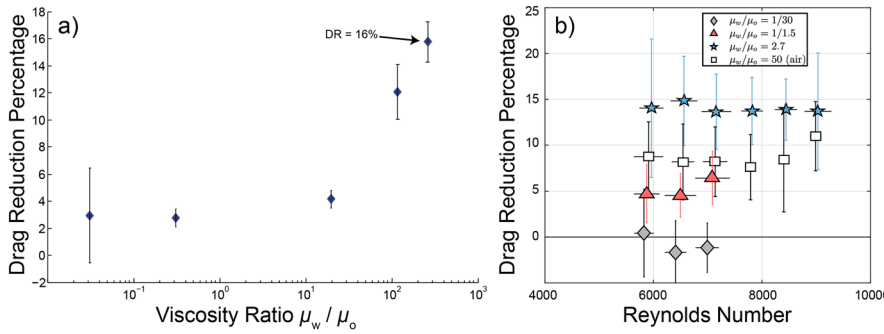

Figure 10.13 (a) Plot of the drag reduction percentage *vs.* the ratio of the working fluid to lubricant viscosity for a laminar flow. Mixtures of water and glycerol are used as the working fluid and a laser-textured sample impregnated with silicone oil is used as the lubricant-impregnated surface. Experiments are conducted in a parallel plate geometry. (b) Plot of drag reduction percentage *vs.* Reynolds number for a variety of working fluid to lubricant viscosity ratios at higher Reynolds numbers. The least viscous lubricant heptane gives a drag reduction percentage of 14%. Experiments are conducted in a Taylor–Couette geometry. Reproduced with permission from Solomon, B. R., Khalil, K. S. & Varanasi, K. K. Drag Reduction using Lubricant-Impregnated Surfaces in Viscous Laminar Flow. *Langmuir* **30**, 10970–10976 (2014).[83] Copyright (2014) American Chemical Society. Reproduced from ref. 85 with permission from AIP Publishing.

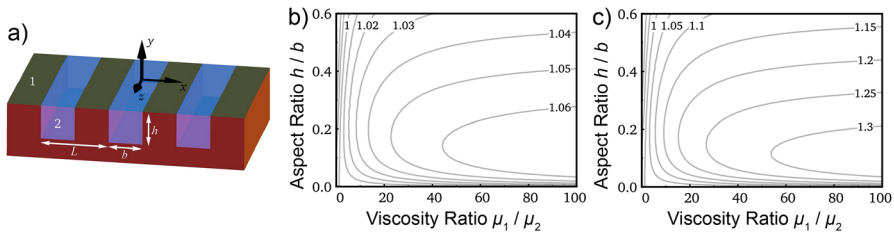

Figure 10.14 (a) Schematic of the analysed lubricant-impregnated surface. Influence of the viscosity ratio on the enhancement factor (given by contours) for longitudinal flow over open grooves with $b/L = 0.98$ where the ratio between the period of the grooves and radius of the channel is (b) 0.02 and (c) 0.1. The enhancement factor is the increased flow rate provided by adding a lubricant-impregnated surface compared to a no-slip condition. C. Schönecker *et al.*, Influence of the enclosed fluid on the flow over a microstructured surface in the Cassie state, *The Journal of Fluid Mechanics*, **740**, 168–195, reproduced with permission.[82]

been measured and rationalized on superhydrophobic surfaces.[87] Jackson points out using simulations that confining lubricants on small scales may lead to additional drag reduction benefits.[88] Wang *et al.* set up an alternate way of measuring drag by spraying surfaces with a controlled flow to measure up to a 7% decrease in drag force on a lubricant-impregnated surfaces.[59]

Drag reduction experiments in Taylor–Couette flows should be extended to Reynolds numbers in excess of 1×10^4. Below this critical Reynolds number, flow instabilities are present in Taylor–Couette flows that prevent the results from being generalized to other geometries.[87,89]

10.3.5 Active Surfaces

Previously discussed motion of drops on lubricant-impregnated surfaces has relied on passive methods, namely the action of gravity. An underexplored area for future work is utilizing active force fields (*i.e.* magnetic, electric, thermal) to manipulate drops. Chen *et al.* have demonstrated that the low hysteresis of lubricant-impregnated surfaces enables drops with magnetic particles to be moved with a magnetic field.[90] More recently, Khalil *et al.* (Figure 10.15a) have created a lubricant-impregnated surface where the lubricant is a superparamagnetic ferrofluid.[91] The lubricant is designed to cloak over drops deposited on the surface, allowing the drops to be manipulated without introducing magnetic particles directly into them. This technique also allows for a wide variety of fluids to be manipulated as long as the lubricant chosen can cloak the working fluid.

Electrowetting, which modifies wetting properties by applying a voltage bias, has emerged as a versatile tool to manipulate droplets of various sizes in a controlled fashion and has been applied to electronic displays, energy

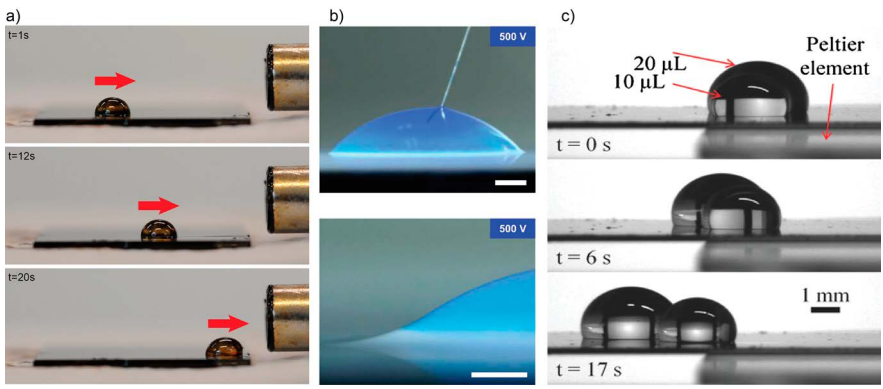

Figure 10.15 (a) A water droplet on a surface impregnated with a ferrofluid moves in response to a magnet. (b) Images of a water drop electrowetted on a lubricant-impregnated surface with an applied voltage of 500 V displaying an apparent contact angle (CA) of ~53°. The bottom image shows the wetting ridge that forms. The scale bar is 400 µm on the top image and 200 µm on the bottom. (c) Simultaneous thermocapillary motion of 10 and 20 µL droplets on a surface impregnated with silicone oil. Reproduced from ref. 91 with permission of AIP Publishing. Reproduced from ref. 95 under the CC BY 4.0 licence. Reproduced from ref. 98 with permission from John Wiley and Sons. Copyright © 2014 Wiley-VCH Verlag GmbH & Co. KGaA, Weinehim.

generation, and microfluidic systems. In a typical system, a voltage between a conducting drop and substrate covered with a dielectric film is applied. Upon application of the voltage, the contact angle of a water drop decreases.[92] When the voltage is removed, contact angle hysteresis can prevent the drop from recovering. Also, severe and uncontrollable droplet oscillations are often encountered. Lubricant-impregnated surfaces have been shown to reduce these undesirable effects as well as reduce any contact angle hysteresis to minimize the reversibility issues, as shown in Figure 10.15b.[47,93–97] Barman *et al.* have also demonstrated that electrowetting two adjacent water drops on lubricant-impregnated surfaces decreases the time it takes them to coalesce by an order of magnitude.[47]

Because liquid surfaces provide extremely low contact angle hysteresis, thermocapillarity can drive the drop along surfaces as shown in Figure 10.15c.[98] Eifert *et al.* remark that the motion can have contributions from thermocapillary forces in the working fluid drop as well as bulk motion of the lubricant but deduce that the motion must be due to thermocapillary forces within the working fluid drop by varying the drop size. Drops on lubricant-impregnated surfaces have also been controlled by changing the local wettability of lubricant-impregnated surfaces.[21,99] The techniques mentioned promise useful for the fabrication of microfluidic designs where a pre-existing microchannel design is not needed.

10.3.6 Optics

Coupling transparency and slipperiness is important for applications ranging from solar modules to commercial eyewear. Superhydrophobic surfaces comprising subwavelength features in transparent materials have shown high transparency while being non-wetting.[100] Lubricant-impregnated surfaces also enable highly transparent and slippery surfaces by reducing the refractive index contrast at the lubricant–air interface in comparison to the original solid–air interface. Several researchers have reported enhancement in broadband optical transmission compared to textured surfaces.[23,26,38,59,90,101,102] Vogel *et al.* demonstrate that the optical transmission through lubricant-impregnated surfaces can surpass that through a glass slide.[23]

Manabe *et al.* point out that even for surfaces with nanoscale features where total transmittance is similar with and without impregnation, lubricant-impregnated surfaces significantly reduce the amount of light scattered.[58] Yao *et al.* impregnated an elastic matrix with a lubricant and showed that the optical transmission can be tuned by deforming the lubricant-impregnated surface.[103]

10.3.7 Infused Gels

A related technology is achieved when for example silicone oil is absorbed by cross-linked solid poly(dimethylsiloxane) (PDMS). The resulting organogel shows slippery properties similar to liquid-impregnated surfaces owing

to the absorbed silicone oil, but unlike a lubricant-impregnated surface the solid texture does not stabilize the silicone oil. Such an infused gel has confusingly been called a lubricant-impregnated surface, but its principle of construction and operation is different from lubricant-impregnated surfaces as described earlier in this chapter.

Surfaces where an organic liquid (*e.g.* silicone oil or Krytox) is infused into a polymer are referred to as organogels.[104–112] Analogously, water can be absorbed by hygroscopic polymers to form a hydrogel.[113–115] It is also possible to create ionic liquid-infused polymer gels.[116,117]

Liquid-infused gels exhibit many similar properties to lubricant-impregnated surfaces including low roll-off of drops,[106,109,110,112,117] anti-icing,[105,113–115,118] enhanced condensation,[119] and anti-biofouling.[107] For example MacCallum *et al.* prevent biofilm accumulation by infusing silicone oil into silicone tubing. They demonstrate by flowing a cultured bacteria solution that the infused silicone tube is devoid of *P. aeruginosa* cells while the control has a large amount of accumulation.[107] Leslie *et al.* also report an infused organogel that prevents thrombosis.[108] Chen *et al.* have also created a hydrogel gel surface and show ice adheres more weakly than superhydrophilic, superhydrophobic, and flat surfaces (Figure 10.16).[113]

10.3.8 Durability

Lubricant-impregnated surfaces show promise in a wide range of applications. For these surfaces to become practically relevant, their durability and robustness should be carefully tested under conditions required by the applications. For example while drop impact has been investigated on

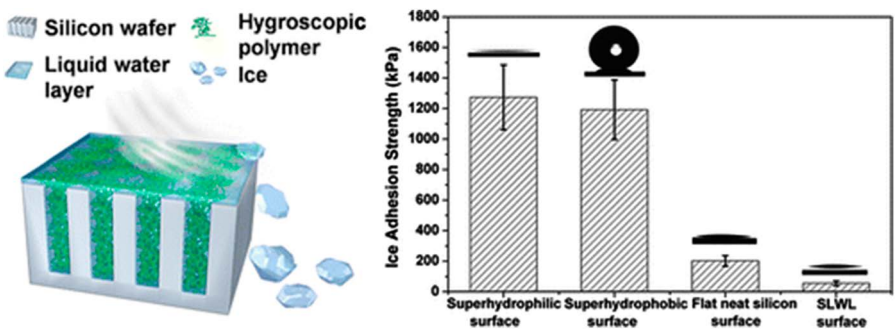

Figure 10.16 Depiction of a microporous silicon filled with a hydrogel. The self-lubricating liquid water layer (SLWL) of the hydrogel surface adheres ice more weakly than superhydrophilic, superhydrophobic, and flat surfaces. Reproduced with permission from Chen, J. *et al.* Robust Prototypical Anti-icing Coatings with a Self-lubricating Liquid Water Layer between Ice and Substrate. *ACS Appl. Mater. Interfaces* **5**, 4026–4030 (2013).[113] Copyright (2013) American Chemical Society.

lubricant-impregnated surfaces,[120,121] under high enough impact conditions an impinging water drop will displace the lubricant and cause the surface to fail. Also, lubricant can be lost from frosting[122] and other phase transitions, but a lubricant source that can replenish the surface over time could overcome this challenge.

In addition, in shear flow Howell *et al.* report that Krytox-impregnated surfaces remain stable under shear flow.[123] However, the work of Wexler, Jacobi, and Stone revealed two mechanisms by which lubricant-impregnated surfaces can fail. In the first, shear forces by an imposed flow can overcome the capillary forces holding the lubricant in place, but cleverly placing non-wetting regions prevent this phenomena from occurring (Figure 10.16a).[124,125] Also, a flow can cause the lubricant to overflow and eventually leave the surface (Figure 10.16b).[126]

As with superhydrophobic surfaces, lubricant-impregnated surfaces are also vulnerable to mechanical failure depending on the strength of the underlying texture. Shillingford *et al.* observe mechanical damage to lubricant-impregnated surfaces made from silica or alumina particles when mechanically abraded that compromises their repellency,[16] hence underlying structures that are robust can overcome this challenge.

LiquiGlide has demonstrated robust lubricant-impregnated surfaces to overcome these durability challenges and has commercialized this technology (see Figure 10.17).[127]

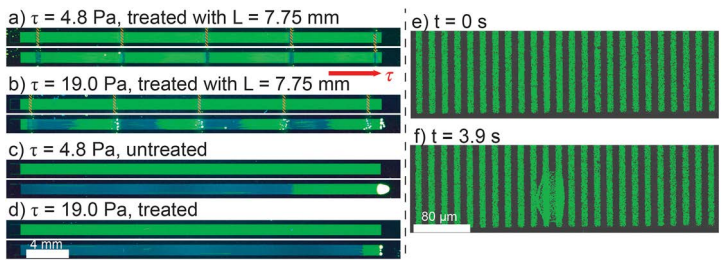

Figure 10.17 Experiments in which a water–glycerol mixture flows over grooves filled with a fluorescent green lubricant. The red arrow indicates the flow direction. The grooves are 9 μm wide, 10 μm deep, and 35 mm long. (a–d) Regions with periodicity L that are non-wetting to the lubricant interrupt grooves aligned with the flow and in (a) prevent drainage of the lubricant. For each experiment, the top image shows the initial state and the bottom the steady state. Drained portions of the groove reflect blue light while excess lubricant appears white. The strength of the imposed flow is characterized by a shear stress τ. (e,f) In a separate set of experiments, at a sufficient stress the flow over lubricant filled groups induces overflow of the lubricant at a shear stress of $\tau = 2.58$ Pa. Reproduced from ref. 125 with permission from The Royal Society of Chemistry. Reprinted from ref. 126 with the permission of AIP Publishing.

10.4 Conclusion and Outlook

Researchers have also begun creating systems iterating on lubricant-impregnated surface technologies to extend their use in new ways. Hou *et al.* have created a liquid-impregnated surface that functions as a membrane to selectively pass gases and liquids,[128] while Sun *et al.* have created a surface that secretes antifreeze upon contact with ice.[129] Dai *et al.* report on a slippery surface comprised of a thin layer of oil trapped in nanoscale textures on a surface of microscale textures. A water drop placed on the surface impales into the texture in a Wenzel-like state but is surprisingly still highly mobile,[130] similar to liquid marbles. McHale and Newton hypothesised that it should be possible to fabricate a liquid-impregnated surface around a liquid drop that would serve microfluidic applications.[131]

Lubricant-impregnated surfaces are a versatile platform that show promise in condensation, anti-icing, anti-fouling, fluid mobility, optics, and drop control. In each application, the design of a lubricant-impregnated surface has particularly relevant criteria of which some are not intuitive. Lubricant-impregnated surfaces can reach commercial applications where superhydrophobic surfaces have fallen short, and may also benefit a multitude of yet undiscovered applications. For example, using the thermodynamic framework,[5] LiquiGlide has designed robust lubricant-impregnated surface coatings and has recently commercialized the technology for manufacturing applications (Figure 10.18).[127]

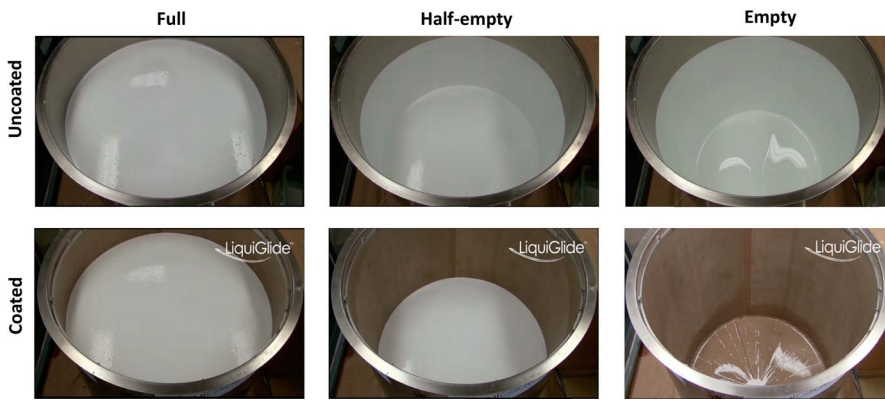

Figure 10.18 Comparison of paint dispensing from a 100 gallon (~400 L) paint mixing tank without (top row) and with (bottom row) the LiquiGlide LIS coating. LiquiGlide coatings demonstrate complete dispensing of the product, saving significant yield loss and reduction in wash water required to clean such tanks. Figure courtesy of LiquiGlide Inc.[127]

References

1. D. Quérék, Non-sticking drops, *Rep. Prog. Phys.*, 2005, **68**, 2495.
2. J. D. Smith, R. Dhiman and K. Varanasi, Liquid-encapsulating surfaces: overcoming the limitations of superhydrophobic surfaces for robust non-wetting and anti-icing surfaces, *64th Annu. Meet. APS Div. Fluid Dyn.*, 2011, **56**, S4.00001.
3. T.-S. Wong, *et al.* Bioinspired self-repairing slippery surfaces with pressure-stable omniphobicity, *Nature*, 2011, **477**, 443–447.
4. A. Lafuma and D. Quéré, Slippery pre-suffused surfaces, *EPL Europhys. Lett.*, 2011, **96**, 56001.
5. J. D. Smith, *et al.* Droplet mobility on lubricant-impregnated surfaces, *Soft Matter*, 2013, **9**, 1772–1780.
6. D. Bonn, J. Eggers, J. Indekeu, J. Meunier and E. Rolley, Wetting and spreading, *Rev. Mod. Phys.*, 2009, **81**, 739–805.
7. J. Zhang, *et al.* Evaporation-induced transition from nepenthes pitcher-inspired slippery surfaces to lotus leaf-inspired superoleophobic surfaces, *Langmuir*, 2014, **30**, 14292–14299.
8. X.-M. Li, D. Reinhoudt and M. Crego-Calama, What do we need for a superhydrophobic surface? A review on the recent progress in the preparation of superhydrophobic surfaces, *Chem. Soc. Rev.*, 2007, **36**, 1350–1368.
9. P. Roach, N. J. Shirtcliffe and M. I. Newton, Progess in superhydrophobic surface development, *Soft Matter*, 2008, **4**, 224–240.
10. F. Schellenberger, *et al.* Direct observation of drops on slippery lubricant-infused surfaces, *Soft Matter*, 2015, **11**, 7617–7626.
11. P. W. Wilson, *et al.* Inhibition of ice nucleation by slippery liquid-infused porous surfaces (SLIPS), *Phys. Chem. Chem. Phys.*, 2012, **15**, 581–585.
12. P. Kim, M. J. Kreder, J. Alvarenga and J. Aizenberg, Hierarchical or Not? Effect of the Length Scale and Hierarchy of the Surface Roughness on Omniphobicity of Lubricant-Infused Substrates, *Nano Lett.*, 2013, **13**, 1793–1799.
13. J. Yang, H. Song, H. Ji and B. Chen, Slippery lubricant-infused textured aluminum surfaces, *J. Adhes. Sci. Technol.*, 2014, **28**, 1949–1957.
14. Y. Tsuruki, M. Sakai, T. Isobe, S. Matsushita and A. Nakajima, Static and dynamic hydrophobicity of alumina-based porous ceramics impregnated with fluorinated oil, *J. Mater. Res.*, 2014, **29**, 1546–1555.
15. Q. Wei, *et al.* Supramolecular Polymers as Surface Coatings: Rapid Fabrication of Healable Superhydrophobic and Slippery Surfaces, *Adv. Mater.*, 2014, 7358–7364.
16. C. Shillingford, N. MacCallum, T.-S. Wong, P. Kim and J. Aizenberg, Fabrics coated with lubricated nanostructures display robust omniphobicity, *Nanotechnology*, 2014, **25**, 014019.

17. M. Raimondo, M. Blosi, A. Caldarelli, G. Guarini and F. Veronesi, Wetting behavior and remarkable durability of amphiphobic aluminum alloys surfaces in a wide range of environmental conditions, *Chem. Eng. J.*, 2014, **258**, 101–109.
18. Y. Takada, M. Sakai, T. Isobe, S. Matsushita and A. Nakajima, Preparation and hydrophobicity of solid–liquid bulk composite using porous glass and fluorinated oil, *J. Mater. Sci.*, 2015, **50**, 7760–7769.
19. Q. Liu *et al.*, Durability of a lubricant-infused Electrospray Silicon Rubber surface as an anti-icing coating. *Appl. Surf. Sci.*, 2015, **346**, 68–76.
20. X. Huang, J. D. Chrisman and N. S. Zacharia, Omniphobic Slippery Coatings Based on Lubricant-Infused Porous Polyelectrolyte Multilayers, *ACS Macro Lett.*, 2013, **2**, 826–829.
21. U. Manna and D. M. Lynn, Fabrication of Liquid-Infused Surfaces Using Reactive Polymer Multilayers: Principles for Manipulating the Behaviors and Mobilities of Aqueous Fluids on Slippery Liquid Interfaces, *Adv. Mater.*, 2015, **27**, 3007–3012.
22. S. Sunny, N. Vogel, C. Howell, T. L. Vu and J. Aizenberg, Lubricant-Infused Nanoparticulate Coatings Assembled by Layer-by-Layer Deposition, *Adv. Funct. Mater.*, 2014, 6658–6667.
23. N. Vogel, R. A. Belisle, B. Hatton, T.-S. Wong and J. Aizenberg, Transparency and damage tolerance of patternable omniphobic lubricated surfaces based on inverse colloidal monolayers, *Nat. Commun.*, 2013, **4**.
24. E. Jenner and B. D'Urso, Wetting states on structured immiscible liquid coated surfaces, *Appl. Phys. Lett.*, 2013, **103**.
25. M. Röhrig, *et al.* Nanofur for Biomimetic Applications, *Adv. Mater. Interfaces*, 2014, **1**, 1300083.
26. P. Zhang, H. Chen, L. Zhang, T. Ran and D. Zhang, Transparent self-cleaning lubricant-infused surfaces made with large-area breath figure patterns, *Appl. Surf. Sci.*, 2015, **355**, 1083–1090.
27. R. Qiu *et al.,* Fabrication of slippery liquid-infused porous surface based on carbon fiber with enhanced corrosion inhibition property, *Colloids Surf. A*, 2014, **453**, 132–141.
28. J. Bico, U. Thiele and D. Quéré, Wetting of textured surfaces, *Colloids Surf., A*, 2002, **206**, 41–46.
29. J. Seiwert, C. Clanet and D. Quéré, Coating of a textured solid, *J. Fluid Mech.*, 2011, **669**, 55–63.
30. K. Rykaczewski, T. Landin, M. L. Walker, J. H. J. Scott and K. K. Varanasi, Direct Imaging of Complex Nano- to Microscale Interfaces Involving Solid, Liquid, and Gas Phases, *ACS Nano*, 2012, **6**, 9326–9334.
31. S. Anand, K. Rykaczewski, S. B. Subramanyam, D. Beysens and K. K. Varanasi, How droplets nucleate and grow on liquids and liquid impregnated surfaces, *Soft Matter*, 2015, **11**, 69–80.
32. F. Schellenberger, Direct observation of drops on slippery lubricant-infused surfaces, *Soft Matter*, 2015, **11**, 7617–7626.

33. Y. Cheng *et al.,* Direct three-dimensional imaging of polymer–water interfaces by nanoscale hard X-ray phase tomography, *Soft Matter*, 2014, **10**, 2982–2990.
34. V. Bergeron and D. Langevin, Monolayer Spreading of Polydimethylsiloxane Oil on Surfactant Solutions, *Phys. Rev. Lett.*, 1996, **76**, 3152–3155.
35. M. E. R. Shanahan and A. Carre, Viscoelastic Dissipation in Wetting and Adhesion Phenomena, *Langmuir*, 1995, **11**, 1396–1402.
36. A. Carre, J.-C. Gastel and M. E. R. Shanahan, Viscoelastic effects in the spreading of liquids, *Nature*, 1996, **379**, 432–434.
37. M. J. Neeson, R. F. Tabor, F. Grieser, R. R. Dagastine and D. Y. C. Chan, Compound sessile drops, *Soft Matter*, 2012, **8**, 11042–11050.
38. J. Zhang, A. Wang and S. Seeger, Nepenthes Pitcher Inspired Anti-Wetting Silicone Nanofilaments Coatings: Preparation, Unique Anti-Wetting and Self-Cleaning Behaviors, *Adv. Funct. Mater.*, 2014, **24**, 1074–1080.
39. S. B. Subramanyam, K. Rykaczewski and K. K. Varanasi, Ice Adhesion on Lubricant-Impregnated Textured Surfaces, *Langmuir*, 2013, **29**, 13414–13418.
40. A. Carlson, P. Kim, G. Amberg and H. A. Stone, Short and long time drop dynamics on lubricated substrates, *EPL Europhys. Lett.*, 2013, **104**, 34008.
41. W. H. Wiser, *Energy Resources: Occurrence, Production, Conversion, Use*, Springer Science & Business Media, 2012.
42. J. W. Rose, Dropwise condensation theory and experiment: A review, *Proc. Inst. Mech. Eng., Part A*, 2002, **216**, 115–128.
43. W. M. Rohsenow, J. P. Hartnett and Y. I. Cho, *Handbook of heat transfer*, McGraw-Hill, New York, 1998, vol. 3.
44. S. Anand, A. T. Paxson, R. Dhiman, J. D. Smith and K. K. Varanasi, Enhanced Condensation on Lubricant-Impregnated Nanotextured Surfaces, *ACS Nano*, 2012, **6**, 10122–10129.
45. R. Xiao, N. Miljkovic, R. Enright and E. N. Wang, Immersion Condensation on Oil-Infused Heterogeneous Surfaces for Enhanced Heat Transfer, *Sci. Rep.*, 2013, **3**.
46. J. B. Boreyko, G. Polizos, P. G. Datskos, S. A. Sarles and C. P. Collier, Air-stable droplet interface bilayers on oil-infused surfaces, *Proc. Natl. Acad. Sci.*, 2014, **111**, 7588–7593.
47. J. Barman, R. Pant, A. K. Nagarajan and K. Khare, Electrowetting on dielectrics on lubricating fluid-infused smooth/rough surfaces with negligible hysteresis, *J. Adhes. Sci. Technol.*, 2016, 1–12.
48. A. Zhang, H. Bai and L. Li, Breath Figure: A Nature-Inspired Preparation Method for Ordered Porous Films, *Chem. Rev.*, 2015, **115**, 9801–9868.
49. K. Rykaczewski, *et al.* Dropwise Condensation of Low Surface Tension Fluids on Omniphobic Surfaces, *Sci. Rep.*, 2014, **4**.
50. M. Cao *et al.,* Water-Repellent Properties of Superhydrophobic and Lubricant-Infused 'Slippery' Surfaces: A Brief Study on the Functions and Applications, *ACS Appl. Mater. Interfaces*, 2016, **8**, 3615–3623.

51. K.-C. Park, S. S. Chhatre, S. Srinivasan, R. E. Cohen and G. H. McKinley, Optimal Design of Permeable Fiber Network Structures for Fog Harvesting, *Langmuir*, 2013, **29**, 13269–13277.
52. B. S. Lalia, S. Anand, K. K. Varanasi and R. Hashaikeh, Fog-Harvesting Potential of Lubricant-Impregnated Electrospun Nanomats, *Langmuir*, 2013, **29**, 13081–13088.
53. L. Cao, A. K. Jones, V. K. Sikka, J. Wu and D. Gao, Anti-Icing Superhydrophobic Coatings, *Langmuir*, 2009, **25**, 12444–12448.
54. S. A. Kulinich and M. Farzaneh, Ice adhesion on super-hydrophobic surfaces, *Appl. Surf. Sci.*, 2009, **255**, 8153–8157.
55. K. K. Varanasi, T. Deng, J. D. Smith, M. Hsu and N. Bhate, Frost formation and ice adhesion on superhydrophobic surfaces, *Appl. Phys. Lett.*, 2010, **97**, 234102.
56. P. Kim, *et al.* Liquid-Infused Nanostructured Surfaces with Extreme Anti-Ice and Anti-Frost Performance, *ACS Nano*, 2012, **6**, 6569–6577.
57. K. Rykaczewski, S. Anand, S. B. Subramanyam and K. K. Varanasi, Mechanism of Frost Formation on Lubricant-Impregnated Surfaces, *Langmuir*, 2013, **29**, 5230–5238.
58. K. Manabe, S. Nishizawa, K.-H. Kyung and S. Shiratori, Optical Phenomena and Antifrosting Property on Biomimetics Slippery Fluid-Infused Antireflective Films *via* Layer-by-Layer Comparison with Superhydrophobic and Antireflective Films, *ACS Appl. Mater. Interfaces*, 2014, **6**, 13985–13993.
59. Y. Wang, H. Zhang, X. Liu and Z. Zhou, Slippery liquid-infused substrates: a versatile preparation, unique anti-wetting and drag-reduction effect on water, *J. Mater. Chem. A*, 2016, **4**, 2524–2529.
60. X. Yin, *et al.* Integration of Self-Lubrication and Near-Infrared Photothermogenesis for Excellent Anti-Icing/Deicing Performance, *Adv. Funct. Mater.*, 2015, **25**, 4237–4245.
61. R. Blossey, Self-cleaning surfaces—virtual realities, *Nat. Mater.*, 2003, **2**, 301–306.
62. A. Lafuma and D. Quéré, Slippery pre-suffused surfaces, *Europhys. Lett.*, 2011, **96**, 56001.
63. T.-S. Wong, *et al.* Bioinspired self-repairing slippery surfaces with pressure-stable omniphobicity, *Nature*, 2011, **477**, 443–447.
64. J. H. Guan *et al.,* Evaporation of Sessile Droplets on Slippery Liquid-Infused Porous Surfaces (SLIPS), *Langmuir*, 2015, **31**, 11781–11789.
65. S. Yang, X. Dai, B. B. Stogin and T. S. Wong, Ultrasensitive surface-enhanced Raman scattering detection in common fluids, *Proc. Natl. Acad. Sci.*, 2016, **113**, 268–273.
66. A. B. Tesler, *et al.* Extremely durable biofouling-resistant metallic surfaces based on electrodeposited nanoporous tungstite films on steel, *Nat. Commun.*, 2015, **6**, 8649.
67. A. K. Epstein, T.-S. Wong, R. A. Belisle, E. M. Boggs and J. Aizenberg, Liquid-infused structured surfaces with exceptional anti-biofouling performance, *Proc. Natl. Acad. Sci.*, 2012, **109**, 13182–13187.

68. A. K. Epstein, T.-S. Wong, R. A. Belisle, E. M. Boggs and J. Aizenberg, Liquid-infused structured surfaces with exceptional anti-biofouling performance, *Proc. Natl. Acad. Sci.*, 2012, **109**, 13182–13187.
69. L. Xiao, *et al.* Slippery Liquid-Infused Porous Surfaces Showing Marine Antibiofouling Properties, *ACS Appl. Mater. Interfaces*, 2013, **5**, 10074–10080.
70. P. Wang, D. Zhang and Z. Lu, Slippery liquid-infused porous surface bio-inspired by pitcher plant for marine anti-biofouling application, *Colloids Surf., B*, 2015, **136**, 240–247.
71. P. Wang, D. Zhang, Z. Lu and S. Sun, Fabrication of Slippery Lubricant-Infused Porous Surface for Inhibition of Microbially Influenced Corrosion, *ACS Appl. Mater. Interfaces*, 2016, **8**, 1120–1127.
72. E. Ueda and P. A. Levkin, Micropatterning Hydrophobic Liquid on a Porous Polymer Surface for Long-Term Selective Cell-Repellency, *Adv. Healthcare Mater.*, 2013, **2**, 1425–1429.
73. R. Steinhagen, H. Müller-Steinhagen and K. Maani, Problems and costs due to heat exchanger fouling in New Zealand industries, *Heat Transfer Eng.*, 1993, **14**, 19–30.
74. S. B. Subramanyam, G. Azimi and K. K. Varanasi, Designing Lubricant-Impregnated Textured Surfaces to Resist Scale Formation, *Adv. Mater. Interfaces*, 2014, **1**, 1300068.
75. T. V. J. Charpentier, *et al.* Liquid infused porous surfaces for mineral fouling mitigation, *J. Colloid Interface Sci.*, 2015, **444**, 81–86.
76. S. Yang, *et al.* Slippery liquid-infused porous surface based on perfluorinated lubricant/iron tetradecanoate: Preparation and corrosion protection application, *Appl. Surf. Sci.*, 2015, **328**, 491–500.
77. T. Song, *et al.* Multiple sheet-layered super slippery surfaces based on anodic aluminium oxide and its anticorrosion property, *RSC Adv.*, 2015, **5**, 70080–70085.
78. T. Song, *et al.* Fabrication of super slippery sheet-layered and porous anodic aluminium oxide surfaces and its anticorrosion property, *Appl. Surf. Sci.*, 2015, **355**, 495–501.
79. J. P. Rothstein, Slip on Superhydrophobic Surfaces, *Annu. Rev. Fluid Mech.*, 2010, **42**, 89–109.
80. C. Ybert, C. Barentin, C. Cottin-Bizonne, P. Joseph and L. Bocquet, Achieving large slip with superhydrophobic surfaces: Scaling laws for generic geometries, *Phys. Fluids*, 2007, **19**, 123601.
81. A. Busse, N. D. Sandham, G. McHale and M. I. Newton, Change in drag, apparent slip and optimum air layer thickness for laminar flow over an idealised superhydrophobic surface, *J. Fluid Mech.*, 2013, **727**, 488–508.
82. C. Schönecker, T. Baier and S. Hardt, Influence of the enclosed fluid on the flow over a microstructured surface in the Cassie state, *J. Fluid Mech.*, 2014, **740**, 168–195.
83. B. R. Solomon, K. S. Khalil and K. K. Varanasi, Drag Reduction using Lubricant-Impregnated Surfaces in Viscous Laminar Flow, *Langmuir*, 2014, **30**, 10970–10976.

84. I. Jacobi, *et al.* Stratified thin-film flow in a rheometer, *Phys. Fluids*, 2015, **27**, 052102.
85. B. J. Rosenberg, T. V. Buren, M. K. Fu and A. J. Smits, Turbulent drag reduction over air- and liquid- impregnated surfaces, *Phys. Fluids*, 2016, **28**, 015103.
86. M. K. Fu and M. Hultmark, *A Model for Turbulent Drag Reduction Over Liquid Infused Micro-textured Surfaces*, European Drag Reduction and Flow Control Meeting – EDRFCM 2015, Cambridge, UK., March 23–26, 2015.
87. S. Srinivasan, *et al.* Sustainable Drag Reduction in Turbulent Taylor-Couette Flows by Depositing Sprayable Superhydrophobic Surfaces, *Phys. Rev. Lett.*, 2015, **114**, 014501.
88. R. L. A. Jackson, Scale Dependent Simulation of Liquid Lubricated Textured Surfaces, *J. Tribol.*, 2010, **132**, 022001–022001.
89. D. P. Lathrop, J. Fineberg and H. L. Swinney, Transition to shear-driven turbulence in Couette-Taylor flow, *Phys. Rev. A*, 1992, **46**, 6390–6405.
90. L. Chen, A. Geissler, E. Bonaccurso and K. Zhang, Transparent Slippery Surfaces Made with Sustainable Porous Cellulose Lauroyl Ester Films, *ACS Appl. Mater. Interfaces*, 2014, **6**, 6969–6976.
91. K. S. Khalil, S. R. Mahmoudi, N. Abu-dheir and K. K. Varanasi, Active surfaces: Ferrofluid-impregnated surfaces for active manipulation of droplets, *Appl. Phys. Lett.*, 2014, **105**, 041604.
92. F. Mugele and J.-C. Baret, Electrowetting: from basics to applications, *J. Phys.: Condens. Matter*, 2005, **17**, R705–R774.
93. H. J. J. Verheijen and M. W. J. Prins, Reversible Electrowetting and Trapping of Charge: Model and Experiments, *Langmuir*, 1999, **15**, 6616–6620.
94. T. Krupenkin, S. Yang and P. Mach, Tunable liquid microlens, *Appl. Phys. Lett.*, 2003, **82**, 316–318.
95. C. Hao, *et al.* Electrowetting on liquid-infused film (EWOLF): Complete reversibility and controlled droplet oscillation suppression for fast optical imaging, *Sci. Rep.*, 2014, **4**, 6846.
96. E. Bormashenko, R. Pogreb, Y. Bormashenko, R. Grynyov and O. Gendelman, Low voltage reversible electrowetting exploiting lubricated polymer honeycomb substrates, *Appl. Phys. Lett.*, 2014, **104**, 171601.
97. M. G. Pollack, A. D. Shenderov and R. B. Fair, Electrowetting-based actuation of droplets for integrated microfluidics, *Lab Chip*, 2002, **2**, 96–101.
98. A. Eifert, D. Paulssen, S. N. Varanakkottu, T. Baier and S. Hardt, Simple Fabrication of Robust Water-Repellent Surfaces with Low Contact-Angle Hysteresis Based on Impregnation, *Adv. Mater. Interfaces*, 2014, **1**, 1300138.
99. I. You, T. G. Lee, Y. S. Nam and H. Lee, Fabrication of a Micro-omnifluidic Device by Omniphilic/Omniphobic Patterning on Nanostructured Surfaces, *ACS Nano*, 2014, **8**, 9016–9024.
100. J.-G. Kim, *et al.* Multifunctional Inverted Nanocone Arrays for Non-Wetting, Self-Cleaning Transparent Surface with High Mechanical Robustness, *Small*, 2014, **10**, 2487–2494.

101. W. Ma, Y. Higaki, H. Otsuka and A. Takahara, Perfluoropolyether-infused nano-texture: a versatile approach to omniphobic coatings with low hysteresis and high transparency, *Chem. Commun.*, 2013, **49**, 597–599.
102. I. Okada and S. Shiratori, High-Transparency, Self-Standable Gel-SLIPS Fabricated by a Facile Nanoscale Phase Separation, *ACS Appl. Mater. Interfaces*, 2014, **6**, 1502–1508.
103. X. Yao, *et al.* Adaptive fluid-infused porous films with tunable transparency and wettability, *Nat. Mater.*, 2013, **12**, 529–534.
104. H. Liu, P. Zhang, M. Liu, S. Wang and L. Jiang, Organogel-based Thin Films for Self-Cleaning on Various Surfaces, *Adv. Mater.*, 2013, **25**, 4477–4481.
105. L. Zhu, *et al.* Ice-phobic coatings based on silicon-oil-infused polydimethylsiloxane, *ACS Appl. Mater. Interfaces*, 2013, **5**, 4053–4062.
106. A. Eifert, D. Paulssen, S. N. Varanakkottu, T. Baier and S. Hardt, Simple Fabrication of Robust Water-Repellent Surfaces with Low Contact-Angle Hysteresis Based on Impregnation, *Adv. Mater. Interfaces*, 2014, 1300138.
107. N. MacCallum, *et al.* Liquid-Infused Silicone As a Biofouling-Free Medical Material, *ACS Biomater. Sci. Eng.*, 2014, **1**, 43–51.
108. D. C. Leslie, *et al.* A bioinspired omniphobic surface coating on medical devices prevents thrombosis and biofouling, *Nat. Biotechnol.*, 2014, **32**, 1134–1140.
109. J. Cui, D. Daniel, A. Grinthal, K. Lin and J. Aizenberg, Dynamic polymer systems with self-regulated secretion for the control of surface properties and material healing, *Nat. Mater.*, 2015, **14**, 790–795.
110. C. Urata, G. J. Dunderdale, M. W. England and A. Hozumi, Self-lubricating organogels (SLUGs) with exceptional syneresis-induced anti-sticking properties against viscous emulsions and ices, *J. Mater. Chem. A*, 2015, **3**, 12626–12630.
111. V. G. Damle, *et al.* 'Insensitive' to Touch: Fabric-Supported Lubricant-Swollen Polymeric Films for Omniphobic Personal Protective Gear, *ACS Appl. Mater. Interfaces*, 2015, **7**, 4224–4232.
112. L. Wang and T. J. McCarthy, Covalently Attached Liquids: Instant Omniphobic Surfaces with Unprecedented Repellency, *Angew. Chem., Int. Ed.*, 2016, **55**, 244–248.
113. J. Chen, *et al.* Robust Prototypical Anti-icing Coatings with a Self-lubricating Liquid Water Layer between Ice and Substrate, *ACS Appl. Mater. Interfaces*, 2013, **5**, 4026–4030.
114. J. Chen, Z. Luo, Q. Fan, J. Lv and J. Wang, Anti-Ice coating inspired by ice skating, *Small*, 2014, **10**, 4693–4699.
115. R. Dou, *et al.* Anti-icing Coating with an Aqueous Lubricating Layer, *ACS Appl. Mater. Interfaces*, 2014, **6**, 6998–7003.
116. Y. Ding, *et al.* Ionic-Liquid-Gel Surfaces Showing Easy-Sliding and Ultradurable Features, *Adv. Mater. Interfaces*, 2015, **2**.

117. D. F. Miranda, *et al.* Physically and chemically stable ionic liquid-infused textured surfaces showing excellent dynamic omniphobicity, *APL Mater.*, 2014, **2**, 056108.
118. Y. Wang, *et al.* Organogel as durable anti-icing coatings, *Sci. China Mater.*, 2015, **58**, 559–565.
119. V. G. Damle, X. Sun and K. Rykaczewski, Can Metal Matrix-Hydrophobic Nanoparticle Composites Enhance Water Condensation by Promoting the Dropwise Mode?, *Adv. Mater. Interfaces*, 2015, **2.**
120. C. Lee, H. Kim and Y. Nam, Drop Impact Dynamics on Oil-Infused Nanostructured Surfaces, *Langmuir*, 2014, **30**, 8400–8407.
121. C. Hao, *et al.* Superhydrophobic-like tunable droplet bouncing on slippery liquid interfaces, *Nat. Commun.*, 2015, **6.**
122. K. Rykaczewski, S. Anand, S. B. Subramanyam and K. K. Varanasi, Mechanism of Frost Formation on Lubricant-Impregnated Surfaces, *Langmuir*, 2013, **29**, 5230–5238.
123. C. Howell, *et al.* Stability of Surface-Immobilized Lubricant Interfaces under Flow, *Chem. Mater.*, 2015, **27**, 1792–1800.
124. J. S. Wexler, I. Jacobi and H. A. Stone, Shear-Driven Failure of Liquid-Infused Surfaces, *Phys. Rev. Lett.*, 2015, **114**, 168301.
125. J. S. Wexler, *et al.* Robust liquid-infused surfaces through patterned wettability, *Soft Matter*, 2015, **11**, 5023–5029.
126. I. Jacobi, J. S. Wexler and H. A. Stone, Overflow cascades in liquid-infused substrates, *Phys. Fluids*, 2015, **27**, 082101.
127. *LiquiGlide Inc*, available at: http://liquiglide.com/.
128. X. Hou, Y. Hu, A. Grinthal, M. Khan and J. Aizenberg, Liquid-based gating mechanism with tunable multiphase selectivity and antifouling behaviour, *Nature*, 2015, **519**, 70–73.
129. X. Sun, V. G. Damle, S. Liu and K. Rykaczewski, Bioinspired Stimuli-Responsive and Antifreeze-Secreting Anti-Icing Coatings, *Adv. Mater. Interfaces*, 2015, **2**, 1400479.
130. X. Dai, B. B. Stogin, S. Yang and T.-S. Wong, Slippery Wenzel State, *ACS Nano*, 2015, **9**, 9260–9267.
131. G. McHale and M. I. Newton, Liquid marbles: topical context within soft matter and recent progress, *Soft Matter*, 2015, **11**, 2530–2546.